Conformational Transitions of Calixphyrin Derivatives Monitored by Temperature-Dependent NMR Spectroscopy. Ab Initio Interpretation of the Spectra

Markéta Bernátková,[*,†,‡] **Hana Dvořáková,**[*,†] **Bruno Andrioletti,**[‡] **Vladimír Král,**[*,†] **and Petr Bouř**[*,§]

Department of Analytical Chemistry and NMR Laboratory, Institute of Chemical Technology, Technická 5, 166 28 Prague 6, Czech Republic, Laboratoire de Chimie Organique, Université P. et M. Curie, Paris VI, UMR7611, 4, place de Jussieu, Tour 44-45, Case 181, Paris Cedex 05, 752 52, France, and Institute of Organic Chemistry and Biochemistry, Academy of Sciences of the Czech Republic, Flemingovo nám. 2, 16610, Praha 6, Czech Republic

Eight *meso*-aryl calixphyrin derivatives were synthesized and their conformational equilibria and transitions studied with temperature-dependent NMR spectroscopy. On the basis of density functional computations, several conformer species could be identified and observed changes in chemical shifts explained. In some compounds, the aryl group rotation and porphyrin ring flipping could be monitored independently, as their NMR coalescence temperatures were well-separated. Calculated relative conformer energies, transition barriers, and isotropic shieldings agree well with the experimental data. In the meso-substituted porhyrins (calixphyrins) the sp^3 carbon atoms perturb their π-electron system and significantly modify the molecular shape and the flexibility. Even when the conjugation of the π-electron system was destroyed by the nonplanarity, far-range electronic induction effects still exist and influence chemical shielding and molecular geometry. The aryl functional groups moderately modify the structure of the calixphyrin ring and thus can be used for fine-tuning of the mechanical and chemical properties of these compounds.

Introduction

Porphyrin derivatives attract attention, because they can be relatively easily modified and usually adopt distinct conformation, and the porphyrin residue often contributes to the stability and ability to enter molecular complexes.[1−3] Binding of ions and small molecules, molecular-recognition chips, and macromolecular structures are some of their typical applications.[4,5]

Calixphyrins (meso-substituted porphyrins), similar to planar porphyrins, can be easily modified by the introduction of various functional groups with distinct positions and orientations toward the porphyrin moiety. Calixphyrins contain a mixture of sp^2 and sp^3 hybridized meso carbon atoms and thus can be viewed as a class of hybrid compounds bearing many features of both porphyrins and calixpyrrols (porphyrinogens); see Figure 1. While for porphyrins the macrocyclic skeleton is fully conjugated through sp^2 bridges, in calixpyrrols, the pyrrole units are bridged by sp^3 meso carbon atoms, and the conjugation is totally disrupted. Apart from being novel structural features, suitable substitution at the carbon bridges can enhance, for example, cation and anion binding properties.[6−10] In vivo, both the reduced (sp^3) and oxidized conjugated (sp^2) forms occur in the porphyrin metabolic pathway. In heme synthesis, for example, the oxidized uroporphyrinogen is decarboxylated and transformed into protoporphyrin,[11,12] while enzyme deficiencies during this process can lead to many diseases, such as the congenial erythropoetic porphyria.[13] The transformation involves
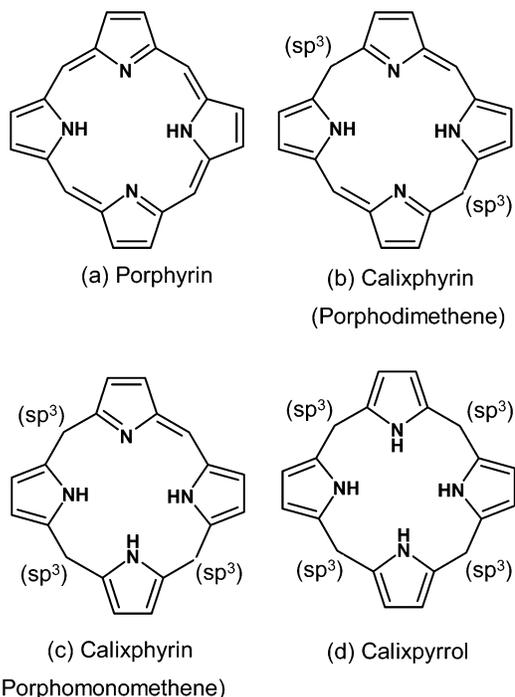

Figure 1. Basic types of the reduced porphyrin group. According to recently introduced nomenclature,[4] the type of (b) of four pyrrol derivatives belongs to calix[4]phyrins-(**1**.*1*.**1**.*1*) as the meso sp^2 and sp^3 carbon atoms alter.

a complicated molecular transfer through the mitochondrial membrane,[14] and the synthetic model systems provide the opportunity to study the molecular flexibility of the partially reduced porphyrin ring in detail.

* To whom correspondence should be addressed. E-mail: mikah@centrum.cz (M.B.); Hana.Dvorakova@vscht.cz (H.D.); vladimir.kral@vscht.cz (V.K.); bour@uochb.cas.cz (P.B.).
† Institute of Chemical Technology.
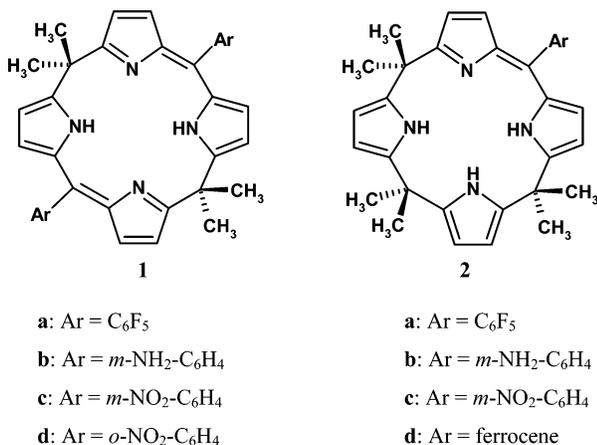‡ Université P. et M. Curie.
§ Academy of Sciences.

Conformational Transitions of Calixphyrin Derivatives

J. Phys. Chem. A, Vol. 109, No. 24, 2005 **5519**

Figure 2. The structures of the studied compounds: **1**, porphodimethenes with two sp^3 meso carbons; **2**, porphomonomethenes of three sp^3 meso carbons.

Recently, synthesis of variously substituted porphodimethenes and porphomonomethenes yielded compounds exhibiting remarkable binding properties.[6−15] Their molecular recognition features can be strongly influenced by sterical demands of the side-chain residues. Also, the geometry and local symmetry of the calix[4]phyrins-(**1**.*1*.**1**.*1*) core itself may vary for molecules differing in substituents not directly attached to the molecular center, as was documented recently by NMR spectroscopy, X-ray diffraction analysis, and quantum mechanical calculations.[15] Because of the applications in macromolecular chemistry, it appears important to understand how the conformations of these compounds can be modified by substituents and how big the energy barriers are that are involved in the conformational changes. In this work, we characterize in detail the molecular motion of a newly synthesized series of sp^2 *meso*-aryl functionalized porphodi- and porphomonomethenes (**1b−d** and **2a−d** in Figure 2, respectively). On this series, the influence of different substituents (nitro vs amino), the calixphyrin-type (mono/dimethene) and ortho/meta substitution can be studied. The rather unusual ferrocene residue was included in order to explore the difference against the usual benzene residue. To some extent, however, the choice was dictated by the limitation in the organic synthesis, and some other compounds did not exhibit enough interesting NMR features to be reported. Note that preparation of these compounds is part of a continuing project aimed at preparation of suitable substances for complex and macromolecular chemistry. Although not all molecular motions were manifested in the NMR experiment, because of limits in accessible temperatures or signal overlapping, the effects of the substituents as well as the different porphyrin cores on molecular flexibility could be independently estimated and compared to theoretical values.

As shown below, because of significant differences in activation energies, indicated also by ab initio computations, the motions of individual molecular parts occur on different time scales and can be studied individually by temperature-dependent ^{1}H NMR experiments. For fast relaxations, local minima on the molecular potential energy surface cannot be further distinguished, and an average signal is measured. Typically, the transition temperature, for which the relaxation speed slows down and individual conformers become detectable, is indicated by broadening and subsequent coalescing (fusion) of NMR spectral lines.[16,17]

Traditionally, molecular structure has been resolved by X-ray crystallography for many porphodimethenes (compounds **1** in Figure 2).[9,18−23] Typically, they adopt a V-shaped conformation

with two approximately planar dipyrromethene units, although a globally planar structure was found in several cases.[15,18] Fewer X-ray structures have been reported for the porphomonomethenes.[24,25] We could crystallize only one of the eight derivatives (**2c**) and report its static structure.[6] In porphomonomethenes, the inverted V (roof-like) shape is distorted, and only one dipyrromethene planar subunit remains. Apart from the difficulties in making crystals, it is not a priori clear how the solid-state data are relevant for solutions and conformational transitions. Thus, we found it useful to complement the present knowledge with the dynamic NMR experiments. Although the NMR technique does not provide atomic resolution, it allows monitoring of dynamic processes in solutions. The information about molecular properties can be further refined if observed data are compared with chemical shifts and conformer energies obtained by ab initio calculations.

Method

Synthesis. Details of the synthesis can be found elsewhere.[6,26] The calix[4]phyrins of type **1** are products of the reaction of 5,5′-dimethyldipyrromethane with the appropriate aldehyde catalyzed by trifluoroacetic acid (TFA) in dichloromethane as solvent. The condensations of the same starting products in propionitrile in the presence of NH$_4$Cl and BF$_3$−Et$_2$O yielded mixtures of calix[4]phyrines of types **2** and **1**, depending on the amount of the aldehyde. The bis- and monoamino derivatives **1b** and **2b** were obtained by reduction of the nitro groups in **1c** and **2c** with hydrazine and palladium on charcoal. The purity of all compounds was validated by NMR, mass spectroscopy, elemental analysis, UV−vis spectroscopy, and IR.

NMR Spectroscopy. The spectra were measured on a Bruker DRX 500 Advance spectrometer operating at 500.1 MHz for ^{1}H and 125.8 MHz for ^{13}C. Chemical shifts are referenced to Me$_4$Si. Typically, spectral width of 7500 Hz, size of 32K data points, recycle time of 3.2, and 16 scans were used. ^{13}C NMR spectra were measured with spectral width of 25 000 Hz, 32K data points, recycle time of 2.7, and 5000 scans. Assignment was accomplished by means of 2D ^{1}H correlation spectroscopy (COSY), 2D ^{1}H−^{13}C heteronuclear multiple-quantum coherence (HMQC), 2D ^{1}H−^{13}C heteronuclear multibond correlation (HMBC), and 1D−dense pulse field gradient spin echo nuclear Overhauser effect (DPFGSE NOE) experiments. 2D COSY was used for resolving ^{1}H spin systems (64 t_1 increments for 1024 (1K) data points, 16 scans, spectral widths 3000−4000 Hz). One- and three-bond ^{1}H−^{13}C connectivities for the assignment of carbon resonances were determined using 2D HMQC (128 t_1 increments for 1K data points, spectral widths 4 kHz (^{1}H) and 22.6 kHz (^{13}C), 64 scans, polarization transfer delay 3.5 ms) and HMBC (128 t_1 increments for 1K data points, spectral widths 4 kHz (^{1}H) and 22.6 kHz (^{13}C), 64 scans, polarization transfer delay) techniques. For dynamic NMR study, temperature-dependent ^{1}H NMR measurements were used. All studied compounds were measured in the temperature range 193−298 K in CD$_2$Cl$_2$ (99.8% D, Merck, Germany). In some cases, the high-temperature measurements were acquired in the range 298−393 K in C$_2$D$_2$Cl$_4$ (99.8% D, Eurorad, Germany). Activation free energies (ΔG^*) were determined using the Eyring equations[27] for the rate constant k

$$k = \frac{k_\mathrm{B} T_\mathrm{C}}{h} \exp\left(-\frac{\Delta G^*}{R T_\mathrm{C}}\right) \qquad (1)$$

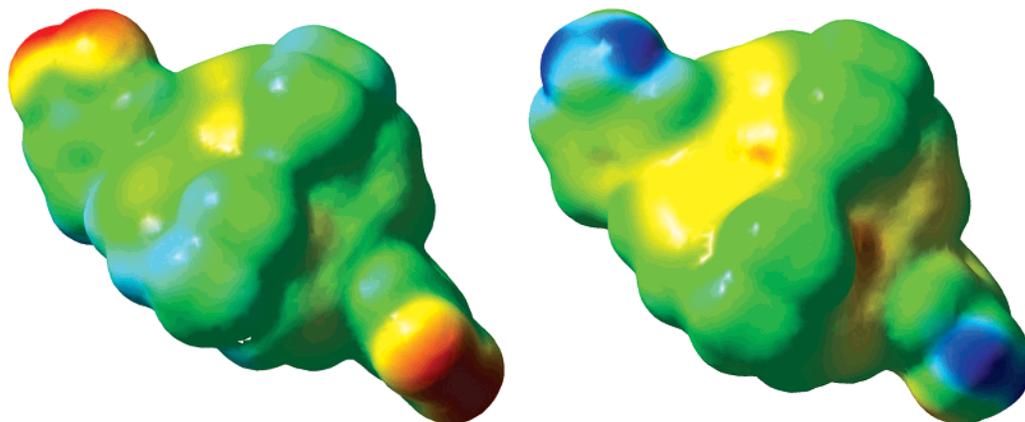$$k = \frac{\pi \Delta \nu}{\sqrt{2}} \qquad (2)$$

Figure 3. Electrostatic potentials on the molecular surface (electron isodensity of 0.0004) of the amino derivative **1b** (left) and the nitro compound **1c** (right).

TABLE 1: Calculated Equilibrium Geometry Parameters for Compounds 1a−d

	α (°)[a]	β (°)[a]	τ (smallest Ar tilt, °)[a]
1a	117	3.7	72
1b	114	7.2	55
1c	115	5.6	58
1d	119	2.5	69

[a] For the meaning of the angles, see Chart 1.

where k_B is the Boltzmann constant, T_C the coalescence temperature, R the gas constant, h the Planck constant, and $\Delta\nu$ the chemical shift difference of the exchanging resonance in the absence of chemical exchange.

Calculations. Equilibrium structures, relative conformer energies, and NMR absolute and relative chemical shifts were obtained ab initio, using the *Gaussian* programs.[28] For fast conformer search, the PM3[29] and HF/4-31G levels were used, while the most stable conformers were investigated with the BPW91/6-31G** level. The general gradient approximation (GGA) BPW91 functional[30,31] does not contain the Hartree−Fock (HF) exchange, which significantly reduces the computational cost. For control calculations, we found that for conformer energies and NMR shifts this level of approximation provides results of comparable quality with the more frequent hybrid B3LYP[32] functional. For selected conformers, the fully optimized structures (BPW91/6-31G**), single-point energies, and NMR shifts were additionally estimated also at the BPW91/6-311++G** level. For the optimized geometries, harmonic frequencies were calculated at the BPW91/6-31G** level, and thus, it could be verified that true minima on the molecular potential energy surface were found. However, we do not include the zero-point vibrational correction in the relative conformer energies, as it is small, and the harmonic approximation may not be relevant for its estimation. The "modredundant" keyword was used for the potential energy scans specified below.

Results and Discussion

Equilibrium Geometries. The equilibrium geometries for compounds **1a−d** were found at the BPW91/6-31G** level as nonplanar, with C_2 symmetry of the calixphyrin four-pyrrole ring. Although the compounds did not crystallize, similar conformation was observed in the X-ray data for a closely related phenyl derivative.[15] Rotation of the aryl substituents obviously disturbs molecular symmetry; however, relative energies of such sub-conformers differ by less than 0.8 kJ/mol and can be considered equivalent because of the expected accuracy of the calculation.
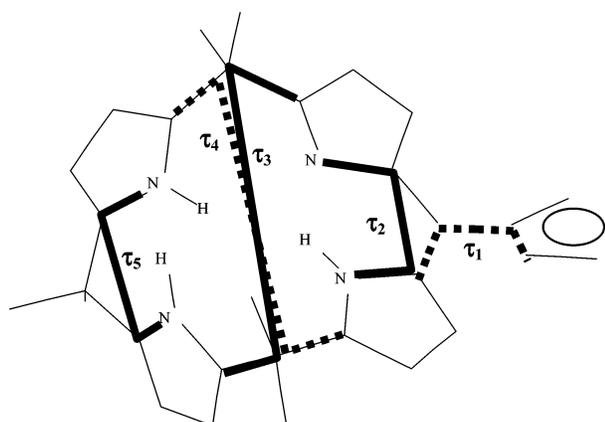
CHART 1: Characteristic Torsional Angles for Compounds 1a−d
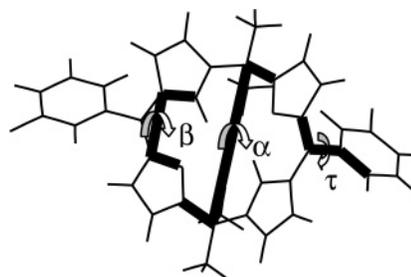
In Table 1, the three torsional angles (α, β, τ; Chart 1) that define the overall molecular shape are listed for equilibrium geometries.

Interestingly, the angles roughly correlate in the mini-series of compounds. For example, for the **1a** derivative, the pentafluorophenyl aromatic residue is most deviated from the pyrrole plane ($\tau = 72°$), which probably disturbs conjugation of the two π-electron systems most. A similar value ($\tau = 69°$) was calculated for **1d**, and both compounds exhibit a bigger value of the ring tilt ($\alpha = 117−119°$) than for **1b** and **1c** where the pyrrole and aromatic parts are more coplanar ($\tau = 55−58°$). The dependence suggests that the less the pyrrole π-electrons conjugate with the aromatics, the more conjugation is possible across the sp³ bridges. This is also confirmed by the angles β, which adopt bigger values (deviation from planarity, 5.6−7.2°) for **1b** and **1c** where the aromatic and pyrrole residues are most conjugated. Obviously, the conjugation is certainly quite limited in comparison with an ideal planar arrangement of the π-electron systems, and the contribution of this phenomenon to the total geometry and energy is supposedly rather small (α angle differences are 2−5°). Note, however, that some calixphyrins can adopt planar conformation even in cases when the π-systems are separated/perturbed by sp³-hybridized carbon.[15]

Little difference in geometry is predicted between the NH_2 and NO_2 substitutions of the aromatic ring (**1b** vs **1c**). This is perhaps somewhat surprising because of the different character of the amino and nitro groups. As can be seen in Figure 3 where the molecular electrostatic potential is mapped on the molecular surface, both groups induce large but opposite local dipoles (with the positive end oriented out and in the phenyl ring for NH_2 and NO_2, respectively).[5] Moreover, the electrostatic field is propagated into the molecular calixphyrin core, which is, for example, dominated by predominantly positive (red/yellow in

Conformational Transitions of Calixphyrin Derivatives

J. Phys. Chem. A, Vol. 109, No. 24, 2005 **5521**

CHART 2: Characteristic Torsional Angles for Compounds 2a−d

TABLE 2: Calculated Equilibrium Geometry Torsion Angles[a] (°) for Compounds 2a−d

	τ_1	τ_2	τ_3	τ_4	τ_5
2a	76	2.5	−159	108	−74
2b	57	2.5	−155	108	−71
2c	60	2.4	−159	110	−74
2d	37	3.0	−136	102	−53

[a] See text, Chart 2, for their definition.

TABLE 3: Coalescence Temperatures (T_c), Activation Free Energies (ΔG^*), and Calculated Transition Barriers (ΔE_{calc}, at the BPW91/6-31G Level) for Aryl and Main Ring Motions**

	ring flipping			aryl rotation		
	T_c [°C]	ΔG^* [kJ/mol]	ΔE_{calc} [kJ/mol]	T_c [°C]	ΔG^* [kJ/mol]	ΔE_{calc} [kJ/mol]
1a	−55	42	35	a	a	134
1b	−35	46	44	a	a	75
1c	−50	43	33	40	68	71
1d	−55	42	38	>135	>82	113
2a	a	a	15[c]	a	a	117
2b	−25[b]	53[b]	21[c]	a	a	79
2c	a	a	15[c]	a	a	71
2d	a	a	27[c]	a	a	27

[a] No transitions were observed within accessible range of temperatures (∼−80...80 °C); supposedly, either the transition temperatures do not lie in this interval or changes in NMR signal were not detectable. Otherwise, the coalescence temperatures were determined to ±5 °C that causes ΔG_0^* to be accurate to ∼1.3 kJ mol^{-1} within the two-state Eyring model. [b] Assignment of this transition to the flipping is rather speculative. [c] Estimated from two subsequent one-dimensional scans along angles τ_3 and τ_5.

the figure) potential for the nitro derivative at the right-hand side of the figure.

For compounds **2a−d**, five torsion angles that characterize the overall conformation are defined in Chart 2.

Similarly to **1a−d**, a distinct tilted (see angles τ_3 and τ_4 in Table 2) equilibrium structure was found, where the two pyrroles connected by the sp^2 carbon are approximately planar ($\tau_2 \approx 0$), while the other two connected with the sp^3 bridges are twisted. The N−H bonds in the latter two pyrroles point alternately above and below an imaginary plane disturbed by the sp^3 carbon ($|\tau_5| \gg 0$). Also, these equilibrium structures may be considered degenerate (within ∼2 kJ/mol) because of the aromatic substituent wagging ($\tau_1 \rightarrow -\tau_1$), calixphyrin ring flipping ($\tau_3 \rightarrow -\tau_3$), N−H hydrogen migration, and movement of the sp^3-bridged pyrroles ($\tau_5 \rightarrow -\tau_5$). As can be seen in Table 2, the pentafluorophenyl substituent (in **2a**) is least coplanar with the

TABLE 4: Selected Experimental and Calculated Relative Chemical Shifts[a]

		experiment				BPW91/6-311++G**			
		σ(¹H)		σ(¹³C)		σ(¹H)		σ(¹³C)	
compound	T [K]	[ppm]		[ppm]		[ppm]		[ppm]	
1b	298	1.96		28.88		1.99		31.28	
	203	1.69	2.10			1.65	2.33	26.72	35.83
1c	363	2.08							
1c (A)	298	1.98		28.80		2.02		31.79	
	193	1.70	2.09	23.97	33.82	1.70	2.35	26.47	36.36
1c (B, C)	298	2.01	1.95	28.15	29.52	2.08	2.05	31.59	
	193	b	b	b	b	1.75	2.37	26.82	36.35
1d (A)	298	1.93		29.13		2.02		31.97	
	183	1.61	2.01			1.70	2.35	27.04	36.9
1d (B)	298	1.78	2.16	25.46	32.90	1.65	2.33	26.49	35.92
	183	1.61	2.18			1.65	2.33	26.49	35.92
2b	298	1.64	1.66	28.84	28.99	1.60	1.64	30.28	31.13
	213	1.56	1.57			1.57	1.60	29.57	30.08
		1.61	1.64			1.62	1.67	30.98	32.18

[a] Calculated standard ¹H and ¹³C TMS shifts were 31.61 and 182.70 ppm, respectively. [b] The species **A**, **B**, and **C** cannot be distinguished at this temperature.

TABLE 5: Relative Energies of the Aryl Rotamers for 1b−d[b]

Conformer (Ar rotamers)		E (kJ/mol) BPW91/6-31G**		
		1b[a]	**1c**	**1d**
A I		1.2 0.8 1.2 0.8	0.8	0.8
A II		0.8 0.4 0.0 0.8	0.0	0.4
B I		1.2 1.6 1.6 0.8	0.4	0.0
B II		0.4 0.4 1.2 0.4	0.0	0.4
C I		1.2 1.5 1.1 0.8	1.2	5.6
C II		1.6 2.0 2.0 1.9	0.4	3.6

[a] Four sub-conformers are possible, due to the pyramidicity of the NH$_2$ group. [b] The pictograms indicate when the aryl substituent points above (solid) or under (dotted line) the paper plane, while the pyrrole planes are approximately perpendicular to the paper; see Figures 5-7 for other graphical representation of conformers **A**−**C**.

pyrrole plane ($\tau_1 = 76°$) and also less that in **1a** (where $\tau = 72°$). For this difference, we cannot see any other explanation than the influence of the distant π-electron pyrrole system, which again suggests some form of electron conjugation over the sp^3 bridges, similarly as for **1a−d**. The ferrocene residue has the cyclopentyl aromatic ring most conjugated with the pyrrole system ($\tau_1 = 37°$) and induces the biggest changes in molecular geometry; overall, however, the geometries of **2a−d** are less sensitive with respect to the aromatic substituents than for **1a−d**, which can be explained by the enhanced flexibility of the molecules caused by the sp^3 connecting carbon atoms.

Molecular Motions. As indicated above, flexibility of the molecules depends on experimental conditions, namely temperature, so that more effective molecular symmetries can be observed in the NMR experiment for the same species. For our compounds, molecular motions with speeds comparable to the NMR time scale include methyl and aryl group rotations, internal N−H tautomerization, and calixphyrin ring distortions. However, not all movements are accessible experimentally. Freezing of the methyl-group rotation was never observed in NMR experiments, where the three hydrogen atoms always provided one signal. The N−H tautomerism was reported for a porphodimethene with a bulky fluorenyl substituent,[15] but we did not observe it for the compounds studied here. This is in agreement with computations (BPW91/6-31G**) predicting a
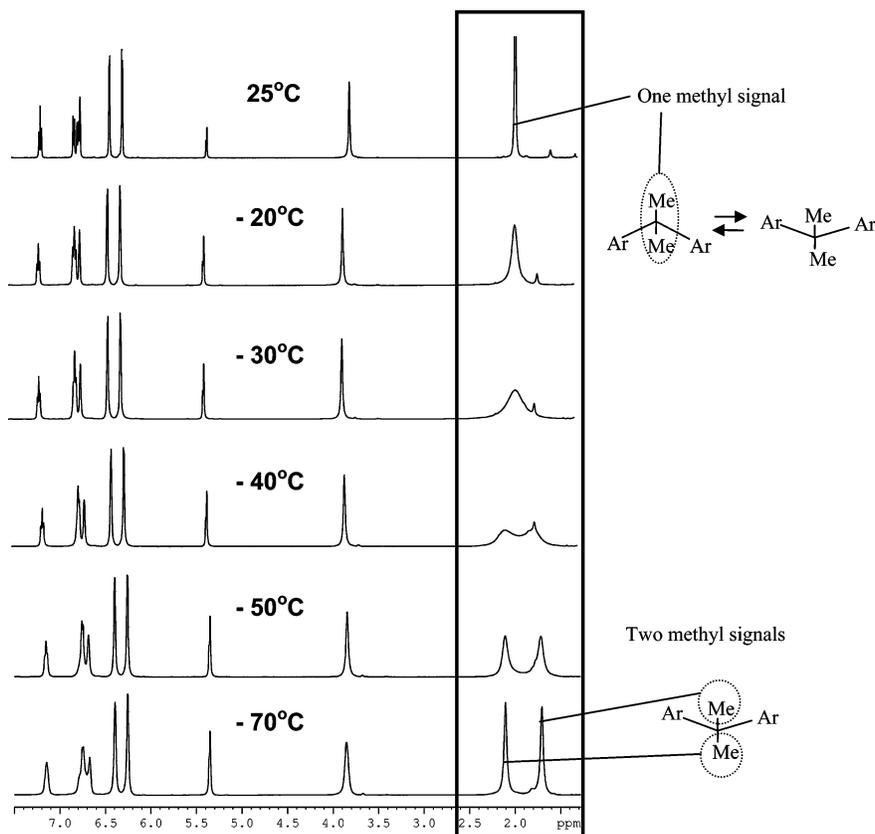
Figure 4. The dependence of the ^{1}H isotropic NMR shift of the **1b** derivative on the temperature (298−193 K) observed in the methyl and aromatic frequency region in CD_2Cl_2 solution.

rather low value of the transitional barriers (<24 kJ/mol) for this process. For example, effective NMR symmetry of the porphodimethene tilted V-shaped conformers becomes C_{2v} due to the tautomerism, and not C_2 as obtained by the calculation for the lowest-energy structure. Trial computations indicate that the motion of the inner hydrogen atoms is accompanied by movements of the porphyrin ring system, including the aryl-group rotation. Indeed, if measurable, the tautomerism was found strongly dependent on the calixphyrin substituents.[15] Obviously, the C_2 structures would have been chiral (enantiomers), and although it is not reasonable to suppose they could be separated, their chirality can be perhaps manifested in complexes with chiral matrixes, as these are often utilized in porphyrin studies.[33] Similarly for the derivatives **2a−d**, more chiral conformers (diastereoisomers) are, in principle, possible because of the tautomerism coupled with the main ring deformations.

However, the aryl rotations and main ring distortions are in some cases accessible to measurement. In Table 3, calculated (BPW91/6-31G**) transition barriers are compiled for all the derivatives and assigned to available experimental coalescence temperatures and activation free energies. Although we did not estimate the entropy contribution, because of the complexity of the problem, we suppose that the free (Gibbs) and calculated potential energies are roughly comparable. Calculated barriers for the rotations of the aromatic residues are relatively high (>71 kJ/mol, except for the ferrocene, see Table 3) and correspond to coalescent temperatures mostly behind the experimentally accessible range. Similarly to the tautomerism, the potential energy scans indicate that the rotation is accompanied by large distortions of the whole molecule. Interestingly, the bulky *ortho*-nitrophenyl ($\Delta E_{calc} = 113$ kJ/mol) group rotates more easily than the perflourophenyl ($\Delta E_{calc} = 134$ kJ/mol) residue. This

can be explained by visualization of the dependence of the molecular geometry on the torsional angle (τ) during the potential energy scan. The calculation thus reveals that the nitro substituent can also rotate (deviate from the benzene ring) and thus enhance passing of the nitro group across the pyrrole rings plane during the aryl rotation. The *meta*-nitro and *meta*-aminophenyl groups exhibit lower barriers of rotation, in both the mono- and dimethenes; however, only in the case of **1c** was it possible to observe it directly in temperature-dependent ^{1}H NMR, as documented in Figure 7 below.

The ring flipping between two V-shaped conformations with approximate C_2 symmetry in **1a−d** is clearly the most easily observable dynamic process within this series, while its barrier is too low for **2a−d** and cannot be observed in most cases. Calculated ring flipping barriers for **1a−d** reproduce the experimental activation energies very well. The theoretical barrier in **2b** was rather underestimated, but in this case, we cannot exclude the point that the coalescence temperature was wrongly assigned to the ring flipping and corresponds rather to the aryl movement or a combination of these motions. All possibilities would produce the fine splitting of the methyl signals (Table 4). Also, for the porphomonomethenes, the two-state one-dimensional transition model may not be valid. For example, the ring flipping (angles τ_3 and τ_4; Chart 2) must be accompanied by the reverse of the twist (τ_5) in order to obtain a conformer of the same energy. Currently, our computational resources do not enable us to study this multidimensional transition by ab initio techniques; in fact, we are not aware of a study that would treat the electronic and vibrational wave function for a similar problem properly. Nevertheless, approximate magnitudes of the transition barriers involved in the ring flipping of **2a−d** could be estimated from subsequent one-
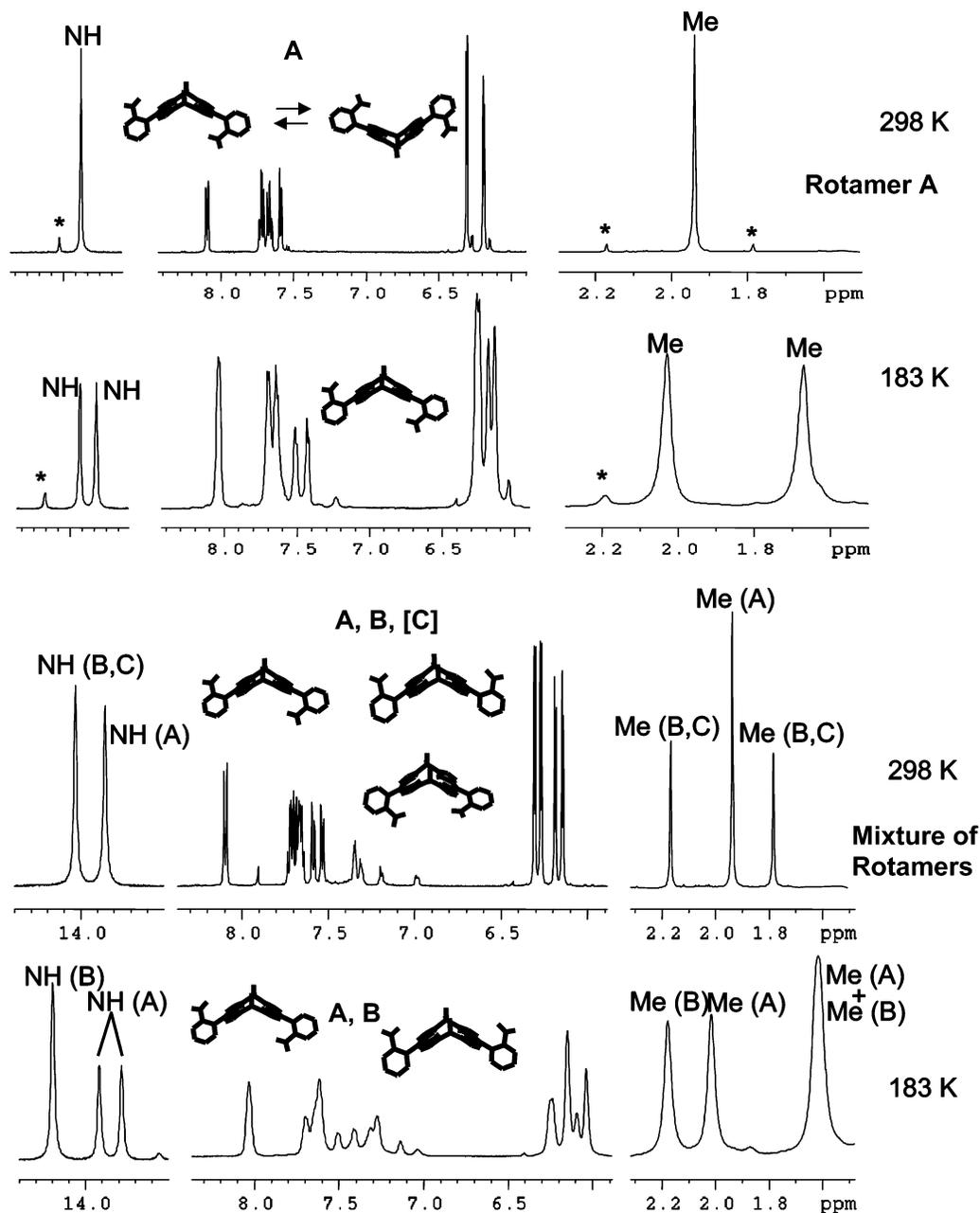
Conformational Transitions of Calixphyrin Derivatives

J. Phys. Chem. A, Vol. 109, No. 24, 2005 **5523**

Figure 5. ^{1}H NMR spectra of the **1d** derivative for 298 and 183 K in CD$_2$Cl$_2$ solution: (top) single rotamer and (bottom) conformer mixture. Traces of rotamer **B** in the experiment with the single conformer are marked by asterisk (*). Occurrence of conformer **C**, however, is less probable because of its higher relative energy.

dimensional scans along the angles τ_3 and τ_5 and are listed in Table 3.

Spectroscopic Manifestation. Despite the structural similarity, the studied compounds behaved quite differently experimentally, and we found the interpretation of their NMR spectra often quite complex. A relatively simple temperature dependence can be seen in Figure 4 for the ^{1}H NMR spectra of the compound **1b.** In the "frozen" state when the ring flipping is slow on the NMR time scale, two signals of the methyl hydrogens are observable at 1.69 and 2.10 ppm, which agrees reasonably well with the values of 1.65 and 2.33 ppm calculated at the BPW91/6-311++G** level; see Table 4. For the elevated (room) temperature, all the methyl hydrogen atoms become "chemically equivalent" with a unique value of the chemical shift (experimentally 1.96, calculated at 1.99 ppm).

The rotation of the aryl moiety in **1a,b** and **2a−d** was not observable in dynamic NMR measurements. Additionally, for

1a and **2a**, the pentafluorophenyl residue is symmetric, and its motion could not influence the NMR spectra. However, the nonsymmetrically substituted aryl groups in the other derivatives can lead, in principle, to NMR-distinct conformer species. The single amino or nitro ortho or meta substituents in compounds **1b−d** appeared to be especially suitable models for the study of this phenomenon. From the calculated relative energies of the rotamers I and II in Table 5, we see that the differences are mostly minor and at the limit of expected accuracy of the computations (∼2kJ/mol). We do not suppose that sub-conformers obtained by wagging of the aryl group (I and II in Table 5) can be distinguished, although they must be considered and averaged in the calculations. For **1c,d**, the predicted activation energies for aryl rotation (71−113 kJ/mol) agree well with the observed data.

The presence of the aryl rotamers **A** and **B** (as classified in Table 5) in the sample is most evident for the *ortho*-nitrophenyl
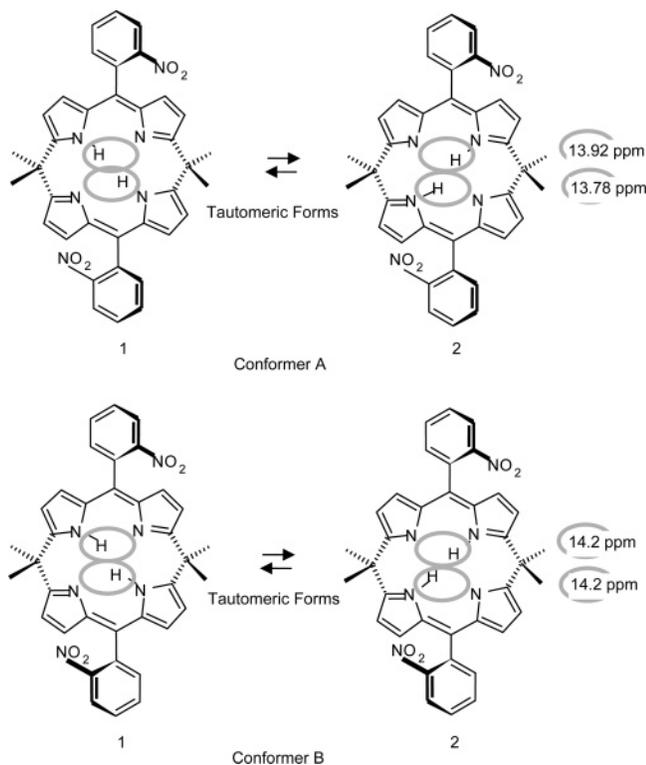
Figure 6. The different NMR signals of the central hydrogens for the rotamers of **1d**. While conformer **A** provides a doublet, the central hydrogen atoms are chemically equivalent for **B** and yield a unique NMR peak. Experimental chemical shifts are indicated in the figure.

substituted calix[4]phyrin **1d**. For **1d**, the relative energy of rotamer **C** is rather high and corresponds to the steric demands and electrostatic repulsion of the nitro groups at the ortho position, while rotamers **A** and **B** have approximately equal energies and should be present in equal ratios in the sample. However, during the isolation procedure, we found it very difficult to separate a mixture of two isomers detectable on thin-layer chromatography (TLC). Rather, we observed only a single compound by measuring ^{1}H NMR in CD_2Cl_2 in the isolated fraction after preparative column chromatography, which was identified as the **A** isomer. Even more interestingly, the equilibration between the **A** and **B** forms is a slow process and can be achieved in several days. For example, a freshly dissolved sample (its spectrum can be seen in the upper part of Figure 5) behaves similarly to the derivative **1b** (cf. Figure 4), and the single peak of methyl hydrogen atoms obtained at room temperature (at 1.93 ppm) splits at 183 K into a doublet (2.01 and 1.61 ppm). However, when the spectrum was remeasured after 5 days of equilibration (at room temperature), new signals appeared at the lower part of Figure 5. Thus, we interpret these observations by supposing that initially only rotamer **A**, where the two NO_2 groups point above and under an imaginary pyrrole rings plane, is present in the sample. For this species, the methyl groups become chemically equivalent under the elevated temperature when the calixphyrin ring flipping is allowed, while at the lowest temperature, two signals can be detected as the tetramethyl system loses its effective D_{2h} symmetry.

Because of the high *ortho*-nitrophenyl group rotation barrier (calculated as 113 kJ/mol, cf. Table 3), rotamers **A** and **B** can be observed individually in the spectrum after the equilibration. Additionally, at the elevated temperature, the equilibrium between isomers **B** and **C** could be easily established, because the **B** → **C** transition involves only the calixphyrin ring flipping ($T_c = -55$ °C, $\Delta G^* = 42$ kJ/mol; Table 3). Although the

calculated relative conformer energy of **C** is high (3.6−5.6 kJ/mol, Table 5) and its molar ratio in the sample is supposedly low, we do not know how this energy difference quantitatively compares with the solution values. The difference in NMR shifts at 298 and 183 K suggest that the real relative energy of **C** is somewhat lower than calculated. For both **B** and **B** + **C** mixtures, the two methyl groups are not chemically equivalent any more, and indeed, we also observe two different methylene resonances at 298 K (Figure 5, Table 4, experimentally at 1.78 and 2.16 ppm).

Strictly speaking, the methyl groups in **B** and **C** are never equivalent, even when the conformers had the same energy, because two of them always lie closer to the NO_2 groups, as the nitro substituents are oriented in the same direction from the molecular center. However, the direct contribution of the NO_2 groups to the methyl hydrogen chemical shifts is rather small (splitting of 0.00 and 0.06 ppm was obtained by trial calculation at the BPW91/6-31G** and BPW91/6-311++G** level, respectively) and cannot explain the observed difference of 0.38 ppm at the room temperature itself. As shown below, a similar type of nonequivalence also becomes observable for the *meta*-nitro derivative **1c**.

This explanation of the behavior of the **1d** compound is in agreement with the shifts observed for the central pyrrole hydrogen atoms. While the **A** conformer has two central nonequivalent hydrogen sites (see Figure 6), these are equivalent for conformers **B** and **C** where the nitro groups point in the same direction. The observed splitting for **A** (0.14 ppm) agrees with the calculated value at the BPW91/6-311++G** level (0.15 ppm,). Heating to 408 K did not change the splitted methyl hydrogen pattern for the **B** and **C** isomers (i.e., the rotation of *ortho*-nitro phenyl ring still remained significantly hindered). The rigidity may be explained by the high calculated energy barrier between these two rotamers, although thermal fluctuations, intermolecular interactions ($\pi-\pi$ stacking), solvent effects, and other factors that cannot be accounted for in the computation can influence the transition as well.

Last, interesting and again unique dynamical behavior among the porphodimethenes could be observed for the *meta*-nitro derivative **1c**, where coalescence temperatures both for the calixphyrin ring flipping as well as for the aryl moiety rotation lie within experimentally accessible range and produce distinct changes in the spectra. As documented in Figure 7, at the highest temperature (363 K), a single hydrogen methyl signal is observed at 2.08 ppm, while it splits for the lowest temperature of 193 K into two signals at 1.70 and 2.09 ppm. This can be explained in an analogy to the *meta*-amino **1b** by the freezing of the calixphyrin ring flipping motion and consequent discrimination of the methyl groups. Additionally, however, at the ambient temperature of 298 K, three sharp, although very close (1.95, 1.98, and 2.01 ppm), methyl signals of a 1:2:1 ratio can be observed. We explain the observation, similarly as for the derivative **1d**, by the hindered aryl-group rotation and consequent presence of several rotamers detectable by NMR. Unlike for the *ortho*-nitro derivative **1d**, rotamers **A**, **B**, and **C** of **1c** have nearly the same energy (cf. Table 5) and thus must be equally populated in the sample. However, as indicated above, methyl groups in **B** and **C** (which behaves as one isomer at 298 K where the calixphyrin rings flips freely, i.e., the conformational exchange is fast on the NMR time scale) are not equivalent, with two of them always pointing in the same direction from the molecular center as the nitro groups. This causes the splitting into the two signals 1.95 and 2.01 ppm, which is close to the calculated values (BPW91/6-311++G**)
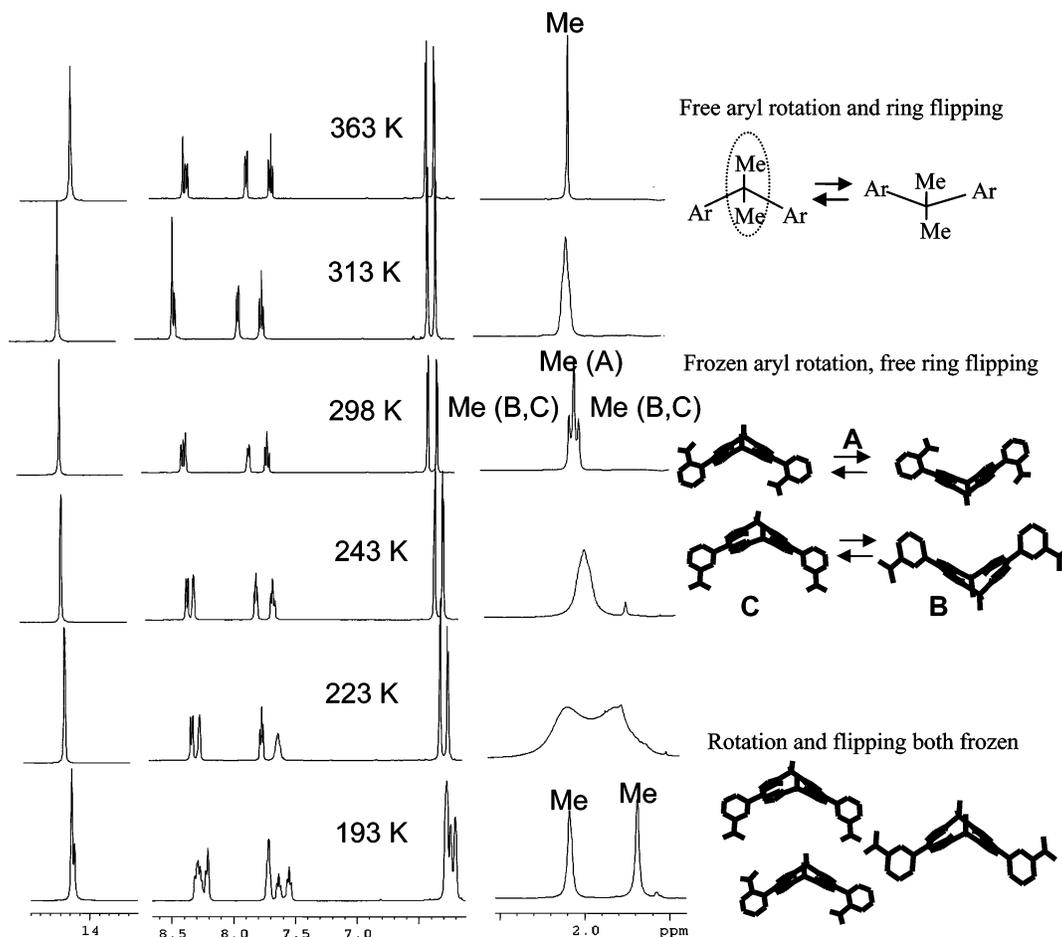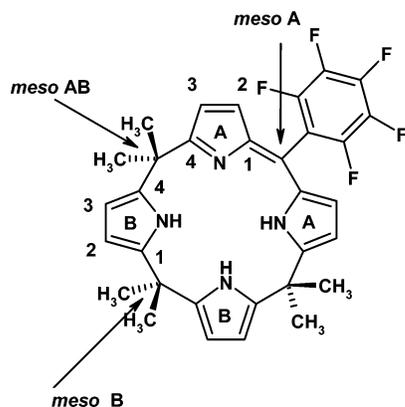
Conformational Transitions of Calixphyrin Derivatives

J. Phys. Chem. A, Vol. 109, No. 24, 2005 **5525**

Figure 7. ¹H NMR temperature dependence of methyl, aromatic, and NH spectral regions of meta-nitro derivative **1c** (CD₂Cl₂ solvent, 298−193 K).

CHART 3: Ring System Notation in 2a

TABLE 6: Selected Experimental and Calculated Nuclear Spin−Spin Coupling Constant (Hz) for 2b−d

compound	J	exp	BPW91/6-31G**	B3LYP/6-31G**
2a	a	4.3	3.95	4.16
	b	3.0	2.04	1.98
2b	a	4.2	3.87	4.07
	b	3.0	2.01	1.96
2c	a	4.2	3.97	4.15
	b	2.9	2.03	2.28
2d	a		3.95	
	b		2.13	

[a] ^3J(H−C=C−H) on pyrroles **A** (see Chart 3). [b] ^4J(H−C=C−N−H) for pyrroles **B**.

of 2.05 and 2.08 ppm. In **A**, where the methyl groups are equivalent, one peak of 1.98 ppm appears (calculated at 2.02 ppm). Assuming that relative conformer energies are equal, the concentration of rotamer **A** is equal to the sum of the concentrations of **B** and **C**, which is consistent with the 1:2:1 signal ratio. The observed coalescence temperature and corresponding $\Delta G°$ (313 K, 68 kJ mol⁻¹) of the aryl rotation is consistent with the calculated energy barrier of 71 kJ mol⁻¹, significantly lower than for the *ortho*-nitro derivative **1d** (Table 3). At low temperature (193 K), either a conformer mixture (**A** + **B** + **C**) is present or one conformer prevails. This cannot be detected, since the nitro group causes minor differences in shifts of methyl atoms (see Table 4, calculated values for **A**, **B,** and **C**), and the signal line width is relatively

broad. However, because of the uneven split of the inner pyrrole hydrogen signal, similarly as for **1d**, we may expect that at least two conformers of **1c** are present in the sample at 193 K. The splitting caused by the influence of the *meta*-nitro is obviously much smaller than for the *ortho*-nitro derivative described in Figure 6.

Hindered rotation of the aryl groups can also be expected for the amino derivative **1b** because of the chemical similarity and similar transition barrier (75 and 71 kJ/mol for **1b** and **1c**, respectively). In this case, we did not observe relevant splitting in the spectra, probably because of the broadening of spectral lines caused by the additional NH₂ out-of-plane bending (nitrogen pyramidicity) isomerization (see Table 5) and a smaller influence of the amino residue on the methyl magnetic shielding. Relative energies of the conformers due to the nitrogen pyramidicity (not shown) were found almost identical (differences were smaller than 1.2 kJ/mol).

The porphomonomethenes **2a**−**d**, because of their greater flexibility, as shown by the energies in Table 3, paradoxically exhibit fewer distinct NMR temperature-dependent features. However, NMR spectroscopy revealed a rather unusual spectral pattern for **2a**−**c** in the aromatic region, where instead of the four doublets characteristic for pyrrole resonances two of them were additionally coupled to a doublet of doublets. This feature could not be observed for the ferrocene derivative **2d** because of signal broadening. The coupling was explained by the COSY spectrum of **2a**, in which two cross-peaks between corresponding pyrrole resonances and an NH proton were detected. This fact, together with observed NOE contacts between meso methyl groups (**AB** in Chart 3) and proton H3 (ring **B**), meso **B** methyl groups and proton H2 (ring **B**), and meso **AB** methyl groups and proton H3 (ring **A**), helped us assign both the pyrrole rings in the conjugated part of the skeleton (rings **A**) and the isolated pyrrole rings adjacent to sp^3 meso carbon bridges (rings **B**).

It is also worth mentioning that relatively intensive four- (or five-) bond long-range interactions both in COSY (between proton H2 (H3) and NH ring **B**) and in HMBC (between proton H2 (H3) of ring **A**) were detected. The assignment of these unusual spin−spin interactions was confirmed by comparison with the coupling constants calculated ab initio using the analytical coupled perturbed method implemented in *Gaussian*.[28,34,35] As can be seen in Table 6, the calculated values are somewhat underestimated, which is, however, acceptable for this level of computation,[34] but the two coupling types (^3J and ^4J) can be clearly distinguished. The existence of such long-range couplings reflects the distinct pyrrole ring arrangements and the π-electron conjugation in the porphomonomethene systems **2a**−**c**. The B3LYP computation, significantly more demanding on computational time than BPW91, systematically improved the ^3J constants, while it did not change the overall accuracy for the longer-range ^4J coupling constants.

Conclusions

The geometry for the eight calixphyrin derivatives as predicted by the ab initio computation was found in agreement with the spectroscopic behavior of the compounds. Additionally, molecular flexibilities as characterized by relative conformer energies and energy barriers for movements of the functional groups could be assessed and verified independently by the computation and subsequent comparison to chemical shifts and conformer barriers determined by temperature-dependent NMR spectroscopy. The substituents, even aryl functional groups relatively distant form the calixphyrin core, significantly modified relative conformer energies, equilibrium geometries, conformational transition barriers, and NMR shielding parameters throughout the whole molecule. We find the possibility to finely tune the properties of the calixphyrin core by the substituents interesting because of the importance of the calixphyrin derivatives for complex and macromolecular chemistry and the relevance to biology.

References and Notes

(1) Sessler, J. L.; Gale, P. A. In *The Porphyrin Handbook*; Kadish, K. M., Smith, K. M., Guilard, R., Eds.; Academic Press: San Diego, CA, 2000; Vol. 6, pp 257−278.

(2) Floriani, C.; Floriani-Moro, R. In *The Porphyrin Handbook*; Kadish, K. M., Smith, K. M., Guilard, R., Eds.; Academic Press: San Diego, CA, 2000, Vol. 3, pp 385−420.

(3) Gale, P. A.; Anzenbacher, P., Jr.; Sessler, J. L. *Coord. Chem. Rev.* **2001**, *222*, 57.

(4) Sessler, J. L.; Zimmerman, R. S.; Bucher, C.; Král, V.; Andrioletti, B. *Pure Appl. Chem.* **2001**, *73*, 1041.

(5) Benech, J.-M.; Bonomo, L.; Solari, E.; Scopelliti, R.; Floriani, C. *Angew. Chem., Int. Ed.* **1999**, *38*, 1957.

(6) Bernátková, M.; Andrioletti, A.; Král, V.; Rose, E.; Vaissermann, J. *J. Org. Chem.* **2004**, *69*, 8140.

(7) Harmjanz, M.; Scott, M. J. *Chem. Commun.* **2000**, *5*, 397.

(8) Bucher, C.; Zimmermann, R. S.; Lynch, V.; Král, V.; Sessler, J. L. *J. Am. Chem. Soc.* **2001**, *123*, 2099.

(9) Bucher, C.; Seidel, D.; Lynch, V.; Král, V.; Sessler, J. L. *Org. Lett.* **2000**, *2* (20), 3103.

(10) Rhe, S. W.; Na, Y. H.; Do, Y.; Kim, J. *Inorg. Chim. Acta* **2000**, *309*, 49.

(11) Battersby, A. R.; Fookes, C. J. R., Matcham, G. W. J., Donald, E. *Nature (London)* **1980**, *285*, 17.

(12) Karlson, P.; Gerok, W.; Gross, W. *Pathobiochemie*; Georg Thieme Verlag: Stuttgart, 1982.

(13) Lehr, P. A.; Doss, M. *Dtsch. Med. Wochenschr.* **1981**, *106*, 241.

(14) Koch, M.; Breithaupt, C.; Kiefersauer, R.; Freigang, J.; Huber, R.; Messerschmidt, A. *EMBO J.* **2004**, *23*, 1720.

(15) Dolenský, B.; Kroulík, J.; Král, V.; Sessler, J. L.; Dvořáková, H.; Bouř, P.; Bernátková, M.; Bucher, Ch.; Lynch, V. *J. Am. Chem. Soc.* **2004**, *126*, 13714.

(16) Sandstrom, J. *Dynamic NMR Spectroscopy*; Academic Press: London, 1982.

(17) Binsch, G. *J. Am. Chem. Soc.* **1969**, *91*, 1304.

(18) Botulinski, A.; Buchler, J. W.; Wicholas, M. *Inorg. Chem.* **1987**, *26*, 1540.

(19) Senge, M. O.; Runge, S.; Speck, M.; Ruhlandt-Senge, K. *Tetrahedron* **2000**, *56*, 8927.

(20) Rhe, S. W.; Na, Y. H.; Do, Y.; Kim, J. *Inorg. Chim. Acta* **2000**, *309*, 49.

(21) Král, V.; Sessler, J. L.; Zimmerman, R. S.; Seidel, D.; Lynch, V.; Andrioletti, B. *Angew. Chem., Int. Ed.* **2000**, *39*, 6.

(22) Bonomo, L.; Solari, E.; Scopelliti, R.; Floriani, C.; Re, N. *J. Am. Chem. Soc.* **2000**, *122*, 5312.

(23) Bischoff, I.; Feng, X.; Senge, M. O. *Tetrahedron* **2001**, *57*, 5573.

(24) Runge, S.; Senge, M. O. *Z. Naturforsch.* **1998**, *53b*, 1021.

(25) Senge, M.; Runge, S.; Speck, M.; Senge, K. R. *Tetrahedron* **2000**, *56*, 8927.

(26) Bernátková, M. Ph.D. Thesis, Institute of Chemical Technology, Prague, 2005.

(27) Leskowitz, G. M.; Ghaderi, N.; Olsen, R. A.; Pederson, K.; Hatcher, M. E.; Mueller, L. J. *J. Phys. Chem. A* **2005**, *109*, 1152.

(28) Frisch, M. J.; Trucks, G. W.; Schlegel, H. B.; Scuseria, G. E.; Robb, M. A.; Cheeseman, J. R.; Zakrzewski, V. G.; Montgomery, J. A., Jr.; Stratmann, R. E.; Burant, J. C.; Dapprich, S.; Millam, J. M.; Daniels, A. D.; Kudin, K. N.; Strain, M. C.; Farkas, O.; Tomasi, J.; Barone, V.; Cossi, M.; Cammi, R.; Mennucci, B.; Pomelli, C.; Adamo, C.; Clifford, S.; Ochterski, J.; Petersson, G. A.; Ayala, P. Y.; Cui, Q.; Morokuma, K.; Malick, D. K.; Rabuck, A. D.; Raghavachari, K.; Foresman, J. B.; Cioslowski, J.; Ortiz, J. V.; Stefanov, B. B.; Liu, G.; Liashenko, A.; Piskorz, P.; Komaromi, I.; Gomperts, R.; Martin, R. L.; Fox, D. J.; Keith, T.; Al-Laham, M. A.; Peng, C. Y.; Nanayakkara, A.; Gonzalez, C.; Challacombe, M.; Gill, P. M. W.; Johnson, B. G.; Chen, W.; Wong, M. W.; Andres, J. L.; Head-Gordon, M.; Replogle, E. S.; Pople, J. A. *Gaussian 98*, revision A.6; Gaussian, Inc.: Pittsburgh, PA, 1998.

(29) Stewart, J. J. P. *J. Comput. Chem.* **1989**, *10*, 209.

(30) Becke, A. D. Exchange-correlation approximations in density-functional theory. In *Modern electronic structure theory*; Yarkony, D. R., Ed.; World Scientific: Singapore, 1995; Vol. 2, pp 1022−1046.

(31) Becke, A. *Phys. Rev. A* **1988**, *38*, 3098.

(32) Becke, A. D. *J. Chem. Phys.* **1993**, *98*, 5648.

(33) Bouř, P.; Záruba, K.; Urbanová, M.; Setnička, V.; Matějka, P.; Fiedler, P.; Král, V.; Volka, K. *Chirality* **2000**, *12* (4), 191.

(34) Bouř, P.; Raich, I.; Kaminský, J.; Hrabal, R.; Čejka, J.; Sychrovský, V. *J. Phys. Chem. A* **2004**, *108*, 6365.

(35) Sychrovský, V.; Gräfenstein, J.; Cremer, D. *J. Chem. Phys.* **2000**, *113*, 3530.